



Ultrasonic characterisation of the elastic properties of mineral aggregates used in asphalt mixtures

Valentin Donev, Olaf Lahayne, Bernhard Pichler & Lukas Eberhardsteiner

To cite this article: Valentin Donev, Olaf Lahayne, Bernhard Pichler & Lukas Eberhardsteiner (2023): Ultrasonic characterisation of the elastic properties of mineral aggregates used in asphalt mixtures, Road Materials and Pavement Design, DOI: [10.1080/14680629.2023.2188090](https://doi.org/10.1080/14680629.2023.2188090)

To link to this article: <https://doi.org/10.1080/14680629.2023.2188090>



© 2023 The Author(s). Published by Informa UK Limited, trading as Taylor & Francis Group



Published online: 19 Mar 2023.



Submit your article to this journal [↗](#)




View related articles [↗](#)



View Crossmark data [↗](#)

Ultrasonic characterisation of the elastic properties of mineral aggregates used in asphalt mixtures

Valentin Donev ^a, Olaf Lahayne ^b, Bernhard Pichler ^b and Lukas Eberhardsteiner ^a

^aInstitute of Transportation, TU Wien, Vienna, Austria; ^bInstitute for Mechanics of Materials and Structures, TU Wien, Vienna, Austria

ABSTRACT

Mineral aggregates are the main constituent of asphalt mixtures by volume, having a significant influence on the performance and durability of asphalt materials and flexible pavements, but their elastic stiffness properties are rarely investigated in the scientific literature. Nevertheless, these properties represent important input to micromechanical models which are aimed at providing a better understanding of the behaviour of asphalt mixtures as the basis for optimising their design. Herein, the elastic properties of 55 cylindrical specimens representing six types of rock from two quarries are investigated using ultrasonic testing, in order to assess the variation of the results between different rock types and between different samples of the same rock type as well as the sensitivity to specimen length (50–150 mm) and frequency (0.05–5.00 MHz). Most of the elastic stiffness values of the investigated rocks are found to be larger than stiffness values frequently used as input to micromechanical models.

ARTICLE HISTORY

Received 6 July 2022
Accepted 1 March 2023

KEYWORDS

Ultrasonic testing; elastic modulus; microstructure; rock materials; micromechanical modelling; X-ray powder diffraction

1. Introduction

The material properties of asphalt mixtures depend on the proportion and the properties of two microstructural constituents: the asphalt binder (bitumen) and the mineral aggregates. Although the asphalt binder makes only 4–5 weight percent of typical asphalt mixtures, it is mostly responsible for their time-, temperature-, and age-dependent properties. Thus, extensive past and ongoing research has been dedicated to achieve a better understanding of the performance and behaviour of asphalt binders. The determination of the rheological properties of bitumen using the dynamic shear rheometer (DSR) has been established as a widely accepted laboratory test method (e.g. AASHTO T315, 2013; EN, 14770 2012). However, the mechanical properties of the mineral aggregates in asphalt mixtures are rarely investigated, and particularly so their elastic stiffness. European standards place requirements on geometrical, physical, chemical and other properties of the aggregates, ensuring that only suitable materials of high quality are used to construct pavements with the necessary performance, durability, and skid-resistance characteristics. Common aggregate tests evaluate gradation, percentage and quality of fines, coarse aggregate angularity, percentage of fractured particles, particle shape characterisation, polishing, Los Angeles abrasion, water absorption, affinity, and others (EN, 13043 2002; Little et al., 2018; Nikolaides, 2015). Nevertheless, the stiffness of the asphalt mixtures increases with increasing stiffness of the aggregate, and this effect becomes particularly important at low temperatures and high loading frequencies.

CONTACT Valentin Donev  valentin.donev@tuwien.ac.at

There are several possible reasons as to why the mechanical properties (e.g. stiffness) of the aggregates are often not investigated. First, the performance of the asphalt mix is mainly dependent on the behaviour of the asphalt binder (Little et al., 2018). The emphasis in current asphalt mix design approaches is on the choice of binder and aggregate gradation, while the selection of specific aggregate type is a question of local availability, in order to keep transportation distances short and, hence, the associated costs low. Second, there is no standard method for the determination of the stiffness of aggregates in asphalt mixes. Third, in contrast to the binder, the aggregate component in the same asphalt mixture might be very heterogeneous due to different aggregate sources (e.g. natural, industrial, recycled), different rock types, different mineral composition (also for the same rock type), and different particle sizes. Consequently, this might be the cause of a significant variation of the mechanical properties within the aggregate phase.

The purpose of the present paper is to provide quantitative experimental access to the elastic properties of several types of aggregate, noting that these properties are required as input to micromechanics models of asphalt mixtures. To achieve this goal, ultrasonic measurements are conducted on 55 rock specimens representing different types of rocks used for the production of asphalt mixtures. Section 2 discusses existing literature reporting the stiffness of mineral aggregates in the context of micromechanical modelling. Section 3 provides a description of the investigated aggregates. Section 4 contains the results of the ultrasonic tests. Section 5 is devoted to a discussion of the findings and their implications for micromechanical modelling of asphalt mixtures.

2. Literature review

The goal of mix and pavement design optimisation is to produce asphalt mixtures and pavements with superior performance regarding common failure mechanisms like fatigue cracking, rutting (permanent deformation) and low-temperature cracking. The complex stiffness modulus is a key parameter used to describe the frequency and temperature dependent material behaviour of different asphalt layers in flexible pavement design. However, the costly and time-consuming laboratory tests for determination of the stiffness of asphalt mixtures are not always feasible or necessary depending on the complexity of the project. For this reason, models for prediction of asphalt stiffness based on the behaviour of the constituents and the volumetric properties of the mix have been the focus of extensive research. The stiffness prediction models can be classified into empirical and mechanistic models. The current mechanistic-empirical design methods for flexible pavements in the USA and Austria (among others) rely on calibrated empirical models for prediction of the complex modulus of asphalt mixtures (AASHTO, 2015; Eberhardsteiner & Blab, 2017). These models are derived using extensive laboratory datasets linking the stiffness of the asphalt mixture to the behaviour of the binder and the volumetric properties of the mix. Many different techniques based on nonlinear regression or machine-learning algorithms were developed during the years to improve the prediction quality of the models or to extend their applicability to new materials and/or larger temperature ranges. The majority of these models consider only the gradation as input regarding mineral aggregates (e.g. Bari & Witczak, 2006; Ceylan et al., 2009; El-Badawy et al., 2018; Golafshani & Behnood, 2018; Gong et al., 2021; Sakhaeifar et al., 2010). Although Singh et al. (2013) included the geometric properties of the aggregates (e.g. shape, angularity, etc.), their study also did not account for the mechanical properties. Notably, the original semiempirical Hirsch model incorporates a fixed aggregate modulus of 29.4 GPa, which was later replaced by a linear regression equation for prediction of aggregate stiffness using solely the aggregate bulk specific gravity as an explanatory variable (Christensen & Bonaquist, 2015).

In contrast to empirical models, mechanistic (multi-scale) models based on the microstructure of asphalt mixtures consider the stiffness properties of both main constituents – bitumen and aggregates. The microstructure-based models can be further divided into numerical finite element or discrete element models (Allen et al., 2017; Arshadi & Bahia, 2015; Coleri et al., 2012; Fakhari Tehrani et al., 2018; Hernandez et al., 2018; Khan et al., 2021; Kollmann et al., 2019; Sawda et al., 2019; You et al., 2008) and analytical continuum-based models using homogenisation theory (Eberhardsteiner

Table 1. Experimentally determined stiffness moduli of aggregates used for asphalt mixtures, as found in the literature.

Rock type	Test method	Aggregate modulus (GPa)	Reference
Limestone 1	Uniaxial compression (0.05–10 Hz)	32–36	You and Dai (2007)
Limestone 2	Uniaxial compression (0.05–10 Hz)	83–88	You and Dai (2007)
Diorite	Ultrasonic	60	Fakhari Tehrani et al. (2018)
Limestone	Ultrasonic	70	Sawda et al. (2019)
Granite	Nanoindentation	58	Barbhuiya and Caracciolo (2017)
Limestone	Nanoindentation	68	Karki et al. (2015)
Basalt	Nanoindentation	55	Yi et al. (2021)
–	Nanoindentation	30	Khan et al. (2021)

et al., 2015a; Kim & Buttlar, 2010; Pichler et al., 2012; Yin et al., 2008; Zhang et al., 2018). Typically, the continuum-based models assume regular geometry of the aggregates (spherical, cylindrical or ellipsoidal), while the finite-element approach allows for more realistic representation of aggregates angularity, shape, and sizes. Regardless of the nature of the used model, the aggregate phase is always modelled as an isotropic linear elastic material.

In the majority of above-mentioned studies, the elastic modulus of the aggregate phase is set to 50–60 GPa and more seldom to 25–30 GPa. The values are based either on assumptions without a specific reference, on typical values from geology textbooks or on a very few studies where the modulus was actually measured. You and Dai (2007) examined two types of limestone through uniaxial compressive tests at frequencies between 0.05 and 10 Hz, obtaining an average complex modulus of 55.5 GPa. Fakhari Tehrani et al. (2018) and Sawda et al. (2019) employed ultrasonic testing and determined an average elastic modulus of 60 and 70 GPa for diorite and limestone samples, respectively. These studies, however, do not provide additional information about the measurements and the evaluation. Furthermore, nanoindentation has gained popularity as a method allowing for the determination of the stiffness values of individual aggregate particles (Barbhuiya & Caracciolo, 2017; Karki et al., 2015; Khan et al., 2021; Yi et al., 2021). A summary of the measured aggregate moduli in these studies are presented in Table 1. In addition, typical values for the mechanical properties of intact rocks are given in Wang (2011). The mean values of the elastic modulus are in the range 29–88 GPa but, according to the author, the values for crushed aggregates produced from these rocks should be higher due to the reduced porosity. Schön (2015) also provides typical values for the mechanical properties of selected rock types as well as wave velocities for both rocks and common rock-forming minerals.

3. Materials

3.1. Specimen preparation

The main goal of this paper is to quantify the absolute values and the variability of the stiffness of mineral aggregates used in asphalt concrete. These stiffnesses are required input to an ongoing micromechanical modelling study which includes more than 45 different asphalt mixtures. Most of these mixtures contain aggregate materials from two quarries in Austria. In the course of the study, large stones were collected from different areas in both quarries with the goal to obtain representative samples from the petrographical point of view. Multiple stones were taken from the same rock type, whereby assumptions about the rock type were based on visual appearance, preliminary information, and the location in the quarry. Subsequently, cylindrical specimens with 50 mm diameter were extracted from the stones in the laboratory using a diamond core drilling equipment. The choice of diameter size was motivated by several factors, including the separation-of-scales requirement (see Section 4.2), limitation of the drilling equipment (smallest possible diameter was 50 mm), and consistency with the scientific literature on ultrasonic testing of rock specimens. The cylinders were then cut to the desired length by means of a sawing machine. From each stone two cylinders with 50 mm



Figure 1. Overview of the produced cylindrical specimens using rock material from two quarries.

length were produced, in order to assess the variation of the stiffness within the same stone. Furthermore, in order to investigate the influence of the specimen length on the ultrasonic measurements, specimens with 100 and 150 mm length were prepared. However, only three specimens with 150 mm length were produced because the cylinders often broke, underlining that only a few stones were suitable for drilling of larger cylinders. A total of 58 rock specimens were produced: 21 specimens from the first quarry where fewer distinct rock types were anticipated, and 37 specimens from the second quarry (see Figure 1). The length and the diameter of each specimen was obtained by taking the average of three measurements at three different positions. The mass density was calculated by dividing the measured mass of the specimen by their volume, whereby the latter was determined using the water displacement method. The unique identifier for each specimen is composed of a Roman numeral, an Arabic numeral, and a letter, specifying the quarry, the stone, and the specimen, respectively. For example, cylinder II-1C originates from the second quarry, the first stone from that quarry, and represents the third specimen produced from that stone.

3.2. Petrographic description

In this paper, the petrographic description of the test specimens is limited to the determination of their mineral composition and the rock classification. Typical natural rock types used in asphalt mixtures include igneous rocks (e.g. gabbro, granite, diorite, diabase, basalt, porphyry), sedimentary rocks (e.g. limestone, sandstone, dolomite), and metamorphic rocks (e.g. gneiss, marble). A petrographic analysis may be conducted using analysis of thin sections, scanning electron microscopy (SEM), X-ray diffraction (XRD), chemical analysis, or other techniques (Wenk & Bulakh, 2004). In the course of this study, an X-ray powder diffraction analysis was performed at the Institute for Applied Geology of the University of Natural Resources and Applied Life Sciences, Vienna (BOKU). X-ray powder diffraction is a method that allows for qualitative and semi-quantitative determination of the mineral composition of rock samples. One of the advantages of XRD is that it can be used to determine the mineral composition of crushed aggregates as well (e.g. filler, sand).

The basic components of an X-ray diffractometer are an X-ray source (X-ray tube), a sample holder, and an X-ray detector (Allmann, 2003; Clearfield et al., 2008; Ermrich & Opper, 2013; Pecharsky & Zavalij, 2009). The method consists of generating X-rays which are directed at the sample, diffracted by the sample phases, collected, and counted by the detector (Figure 2). Diffraction occurs only at a specific angle that is dependent on the unique crystal structure of the mineral (i.e. the atomic arrangement in the unit cell). An X-ray diffractogram (diffraction pattern) is obtained as a plot of the intensity of the diffracted X-rays (ordinate) versus a varying diffraction angle 2θ (abscissa). In the standard Bragg–Brentano geometry, the diffraction angle can be changed, for example, by rotating both the X-ray tube and the detector, while the sample remains fixed (θ/θ mode). The position, intensity and profile of the individual peaks in the diffractogram are used for detection of mineral phases by searching in a standard reference database. Nevertheless, the correct determination is often dependent on additional information about the samples and the experience of the investigator.

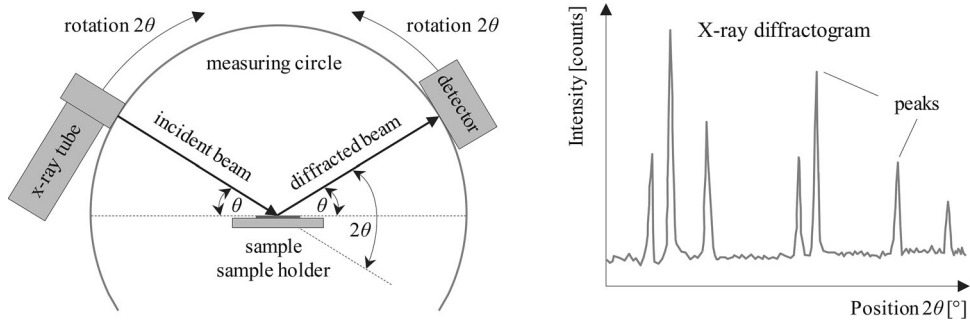


Figure 2. Principle setup of a standard Bragg-Brentano X-ray diffractometer in a θ/θ mode (left) and diffraction pattern composed of multiple Bragg peaks (right).

Table 2. Mineral composition for six rock samples determined by X-ray powder diffraction with deduced rock type.

Specimen	Mineral constituents				Rock type	Similar to
I-6	Dolomite	96%	Quartz	< 0.5%	Dolomite	I-1, I-2, I-3, I-4, I-5
	Calcite	2%	Muscovite	< 0.5%		
	Feldspar	1%				
I-8	Calcite	93%	K-feldspar	1%	Limestone	I-7, I-9
	Dolomite	4%	Quartz	< 0.5%		
	Muscovite	1%	Goethite	< 0.5%		
II-2	Dolomite	84%	Biotite	1%	Dolomitic Marble	II-1, II-3, II-4
	Calcite	11%	Garnet	1%		
	Olivine	2%	Diopside	< 0.5%		
	Lizardite	1%				
II-5	Plagioclase	30%	Quartz	14%	Kersantite (lamprophyre)	II-6
	K-feldspar	19%	Augite	4%		
	Amphibole	18%	Chlorite	< 0.5%		
	Biotite	16%				
II-7	Quartz	33%	Plagioclase	12%	Gneiss	II-8, II-9
	K-feldspar	17%	Garnet	9%		
	Sillimanite	17%	Chlorite	< 0.5%		
	Biotite	13%				
II-11	Plagioclase	39%	Garnet	8%	Gneiss	II-10
	Quartz	26%	Amphibole	6%		
	Biotite	21%	Kyanite	< 0.5%		

In the course of this study, additional samples were drilled from six selected stones. The samples were crushed, dried at 70°C, homogenised and milled to a fine powder with a particle size not larger than 20 μm . The measurements were conducted with Panalytical X'Pert Pro MPD diffractometer with automatic divergence slit, Cu LFF tubes (45 kV, 40 mA), and an X'Celerator detector. The data was collected at 2θ from 2° to 70° with a step size of 0.017° and measurement time of 25 s per step. The semi-quantitative determination of the mineral composition was conducted according to the Rietveld method with the software Panalytical X'Pert HighScore Plus. The Rietveld refinement consists of generating a theoretical diffractogram of all detected phases based on their characteristic structure data. By minimising the sum of the squared deviations between the experimental and the theoretical diffractogram, a quantification of the mineral phases is possible (Clearfield et al., 2008; Pecharsky & Zavalij, 2009). The results for the six samples are presented in Table 2 listing the detected minerals in each rock specimen together with their weight fractions. The detection limit was about 1% by weight. The rock type in the penultimate columns was determined based on the mineral composition and the texture of the rock.

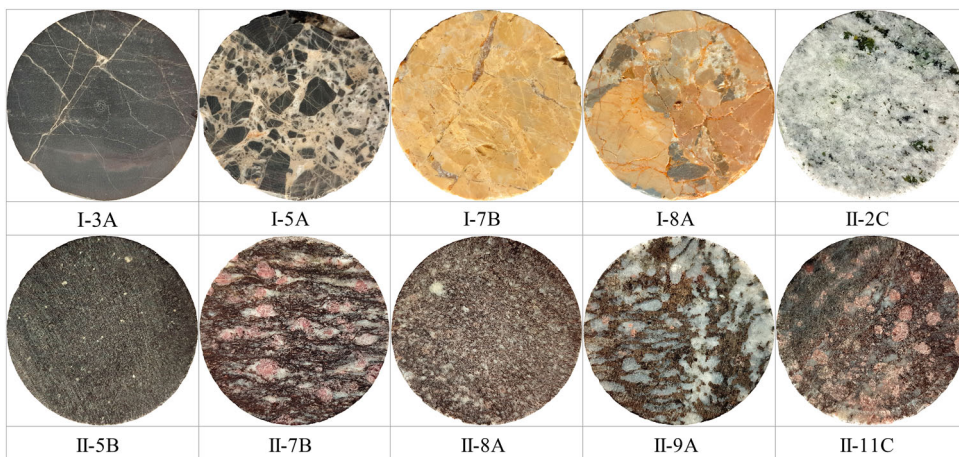


Figure 3. Top view of selected cylindrical specimens (50 mm diameter). The surface of the specimens was wetted with water for a better contrast.

The visual appearance of rock specimens is shown in Figure 3, allowing inferences to be made regarding colour, homogeneity, texture, porosity, and degradation state. Samples I-1 to I-6 are classified as the sedimentary rock dolomite (dolostone). Specimen I-3A appears like a homogeneous, fine-grained rock with dark grey-blue colour (see Figure 3). In contrast, stone samples I-5 and I-6 exhibit dark grey grains of various sizes which are scattered in a light-grey matrix. The difference can most likely be attributed to variable calcite content. This rock type was rather prone to cracking during drilling, rendering the preparation of specimens quite difficult. The visible cracks and white veins (calcite) are expected to influence the overall mechanical properties. Dolomite is slightly harder than limestone but it still has low polishing value which limits the use of dolomite aggregates in Austria to the base and binder asphalt concrete layers (e.g. Hofko et al., 2011).

The rock type of stone samples I-7 to I-9 is clearly limestone (sedimentary). The XRD results of sample II-8 reveal a monomineralic rock with 93% calcite and 4% dolomite. The colour of the specimens is between off-white and yellow. It can be expected that some specimens like II-7B exhibit even higher calcite percentage and less impurities (see Figure 3). All limestone specimens are characterised by higher porosity in comparison to the other rock types and visible cracks. Limestone is a soft rock with low polishing resistance and large water absorption. In Austria, limestone is commonly used as a filler in asphalt mixtures.

Sample stones II-1 to II-4 are classified as dolomitic marble which is the metamorphic equivalent of dolomite. In comparison to the latter, the dolomitic marble samples exhibit light grey colour and larger average grain size. The predominant mineral in the examined sample from stone II-2 is dolomite followed by calcite (colourless, shiny grains). Detected impurities include biotite (dark), garnet (red) as well as olivine, diopside, and lizardite (green). Their percentage (5% in II-2) appears to vary across the different specimens.

The rock type of sample stones II-5 to II-6 is kersantite, an igneous rock with a medium to dark colouring and fine-grained minerals, as can be seen in Figure 3 (II-5B). Despite the homogeneous appearance, this is a polymineralic rock with primary constituents: feldspars (plagioclase and K-feldspar, light colour), amphibole (dark), biotite (dark), and quartz. Aggregate made from kersantite is regarded as a high-quality product and often used in asphalt surface layers.

Sample stones II-7 to II-11 can be roughly classified as the metamorphic rock gneiss. The main mineral components are feldspars, quartz, biotite, and garnet. Stone II-7 contains sillimanite (white) and stone II-11 (II-10 is like II-11) contains amphibole. Stones II-8 and II-9 can also be classified as gneiss but the exact mineral composition is unknown as they were not investigated using powder diffraction.

These two samples are different with regard to their texture. Stone II-8 is fine to medium-grained, whereas stones II-9, II-10, and II-11 are course-grained. Samples II-7 and II-9 exhibit alternating light and dark colour banding.

A more precise petrographic description would require X-ray diffraction analysis of all specimens and eventually analysis of thin sections using polarising microscope. However, the determination of the exact mineral composition would require high efforts and destruction of the specimens, while the benefit for the purpose of this study would be small. Moreover, the mechanical properties of rocks depend not only on the qualitative and quantitative mineral composition (i.e. the mechanical properties of the minerals) but also on a number of other factors like density, porosity, grain size, the degree of weathering, defects (microcracks, grain boundaries), structure, and the texture of the rock (interlocking, tendency to fracture along layers, etc.). In the next section, the results of the ultrasonic tests are presented.

4. Ultrasonic tests

4.1. Test method overview

Sound waves with frequencies larger than the human hearing range (> 20 kHz) are called ultrasonic. Ultrasonic testing is a non-destructive test method with many engineering applications including flaw detection, dimensional measurements, quality control, and material characterisation. The method consists of sending ultrasonic waves through a material, which are then detected and analysed (see Krautkrämer & Krautkrämer, 1990). The very small stresses which are induced in the tested medium allow for assuming a linear relationship between stresses and strains. Moreover, the velocity of ultrasonic waves at a given temperature and pressure represents a characteristic material property.

The ultrasonic testing equipment consists of a display device (oscilloscope), a pulser-receiver, and transducers (Figure 4). In the here employed through-transmission method, the pulser-receiver produces electrical pulses which are converted to a sound wave by the transducer (acting as a sender). The sound wave propagates through the sample and is then converted back to an electrical signal by the transducer (acting as a receiver) at the other end of the specimen. The pulser-receiver amplifies and conditions the signal for the oscilloscope. The choice of transducers depends on the frequency and the types of waves that should be produced (longitudinal or transversal). As for longitudinal (compression) waves, the movement of material particles is in the same direction as the direction of propagation of the wave. As for transversal (shear) waves, the movement of material particles is orthogonal to the direction of wave propagation. A coupling agent in the form of a thin film between the transducer and the specimen facilitates the transmission of sound energy. For the same reason, the surfaces of the specimen should be as smooth as possible. In order to achieve high-quality transmission of shear waves, the coupling agent should exhibit a significant viscosity. An auxiliary device with two clamps

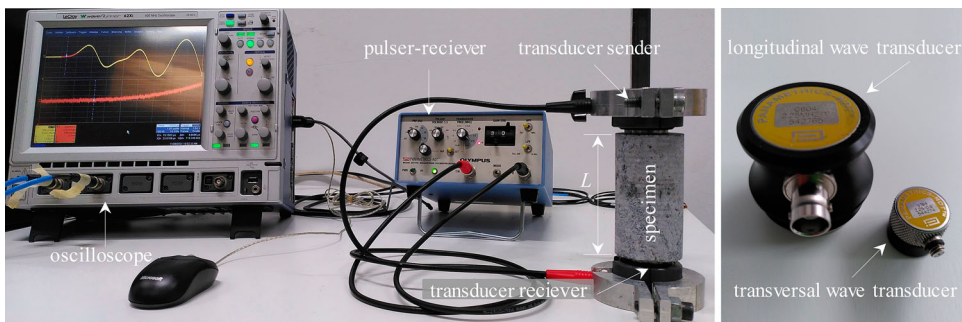


Figure 4. Used ultrasonic measuring equipment with oscilloscope, pulser-receiver, transducers, auxiliary transducer holding device, and specimen (left) and transducers for longitudinal and transversal waves with 2.25 MHz frequency (right).

can be employed to fix the positions of the transducers. The used equipment in this study consists of a Panametrics pulser-receiver 5077PR, a digital oscilloscope Lecroy WaveRunner 62Xi, and piezoelectric transducers Panametrics.

The main result of the ultrasonic test for determination of stiffness is the time of flight through the specimen which must be determined for both longitudinal and transversal waves. To get the exact times of flight for the rock specimen, the system delay time (t_0) has to be measured and subtracted from the total travel time (t_{tot}). The system delay time is the travel time without the specimen considering the delay caused by the transducer and the coupling agent (honey).

In the following, the essential formulas for quantification of the elastic stiffness properties based on ultrasonic testing are presented. Details on the theoretical foundations and the derivation of the formulas can be found in the literature (e.g. Carcione, 2014; Kohlhauser, 2009). The velocities of the longitudinal (v_L) and the transversal waves (v_T) can be determined using the corresponding arrival times ($t_{L,tot}$ and $t_{T,tot}$) and the length of the specimen which equals the travel distance (L) as follows:

$$v_i = \frac{L}{t_i} = \frac{L}{t_{i,tot} - t_{i,0}} \quad (1)$$

The wavelength (λ_i) can be then computed using the frequency (f) according to the following equation:

$$\lambda_i = v_i/f \quad (2)$$

This equation reveals a significant advantage of ultrasonic testing, namely that by changing the frequency it is possible to characterise the material at different length scales. However, when selecting the frequency, the separation of scales requirement should be satisfied (see Section 4.2.). As for the evaluation of test results based on the theory of wave propagation through linear elastic media, the type of the wave travelling through the investigated material must be known: (i) longitudinal *bulk* waves are similar to waves propagating through infinite media (prevented lateral deformation), (ii) longitudinal *bar* (extensional) waves are similar to waves propagating through slender rods (free lateral deformation). In contrast to these two categories, the propagation of transversal waves is significantly less affected by the geometric properties of the tested specimen (Aydin, 2013; Kohlhauser, 2009). Thus, for an isotropic homogeneous elastic material, the longitudinal bulk wave velocity v_L (the transversal wave velocity v_T) is related to the stiffness tensor component C_{1111} (C_{1212}) and the mass density ρ through:

$$v_L = \sqrt{\frac{C_{1111}}{\rho}}; \quad v_T = \sqrt{\frac{C_{1212}}{\rho}} \quad (3)$$

The elastic modulus (E) and Poisson's ratio (ν) can be computed using

$$E = \rho \times \frac{v_T^2 \times (3 \times v_L^2 - 4 \times v_T^2)}{v_L^2 - v_T^2}; \quad \nu = \frac{v_L^2 - 2 \times v_T^2}{2 \times (v_L^2 - v_T^2)} \quad (4)$$

It follows from the formula for Poisson's ratio that the time of flight of a transversal wave is 1.5–2.0 times longer than that of a longitudinal wave, provided that Poisson's ratio of the characterised isotropic material is within the interval from 0.10 to 0.33. Furthermore, the bulk modulus (K) and the shear modulus (G) can be obtained by

$$K = \frac{\rho}{3} \times (3 \times v_L^2 - 4 \times v_T^2); \quad G = \rho \times v_T^2 \quad (5)$$

Equation (5) reveals that the shear modulus depends only on the transversal wave velocity, whereas the bulk modulus depends on both the velocity of longitudinal and transversal waves.

The determination of flight times is best explained on the basis of an example. The top graphic of Figure 5 shows an output signal caused by a transversal wave transducer with 2.25 MHz frequency.

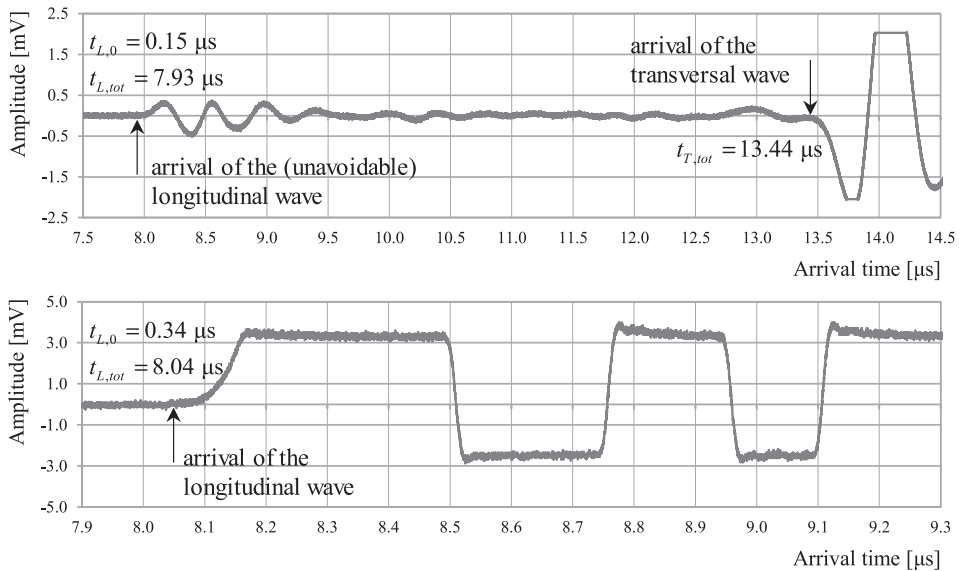


Figure 5. Example of arrival time detection and measured ultrasonic signal caused by transversal (top) and longitudinal (bottom) wave transducers with frequency of 2.25 MHz for rock specimen II-6B.

It can be seen that a preceding low-amplitude longitudinal wave cannot be completely avoided. The time of flight can be read manually on the oscilloscope as the time of the first arrival of the ultrasonic wave which is the time when the signal deviates from the noise (Kohlhauser & Hellmich, 2013). A better signal for determination of the arrival time of longitudinal wave can be obtained by using a transducer for longitudinal waves with the same frequency (Figure 5, bottom). Thus, the arrival times of longitudinal waves in this study were determined twice for all specimens, namely once with a transducer for longitudinal waves and once with a transducer for transversal waves. With the exception of a few obviously damaged samples, the difference in the determination of flight time was less than 1%. Determination of the time of arrival of transversal waves is more difficult and prone to subjectivity depending on the quality of the signal of the longitudinal wave, which arrives before the signal of the transversal wave.

In a perfect homogeneous medium, the ultrasonic waves would propagate purely according to the principles of elastic materials without any reflection (wave bounces off at a smooth boundary), diffraction (change of direction when passing through/around an obstacle), or diffusion (scattering at a rough boundary). Inhomogeneous media, though, can contain voids, defects, grain boundaries, or other obstacles which influence the propagation of the elastic waves depending on their size and geometry and which can cause reflection, diffraction, and/or diffusion, thus diminishing the signal quality. In the here conducted tests, the sender and the receiver of the ultrasonic signals were aligned parallel to each other on the opposite ends of the cylinders. Therefore, based on Huygen's principle, reflections, diffraction, diffusion, and/or interference within the sample do not change the alignment of the wavefronts of the signal component running parallel to the symmetry axis (Krautkrämer & Krautkrämer, 1990). Relevant for stiffness characterisation is the *time of arrival* of the front of each ultrasonic pulse at the receiver (see the marked positions of the pulse fronts in Figure 5). This time is determined by the signal component running parallel to the axis and therefore it is not influenced by reflection, diffusion, and/or diffraction. These phenomena, though, do influence the *amplitude* of the signal between the arrival of the longitudinal and that of the transversal wave and can disimprove the clearness of the pulse fronts. As can be seen in the given example, the amplitude of the signal of the unreflected component was significantly higher than the amplitude of any reflected or diffracted component, which

can be attributed to the choice of the frequency, the dimensions of the samples, and their painstaking preparation.

4.2. Sensitivity to ultrasonic frequency

Next, the selection of specimen geometry and ultrasonic frequency is discussed. As described in Section 3.2, the rock specimens exhibit a heterogeneous microstructure consisting of individual mineral grains with likely different mechanical properties. However, the complex microstructure can be replaced by a macro-homogeneous representative volume element (RVE) with spatially constant effective stiffness properties (representative for the material), as long as two conditions are satisfied. First, the heterogeneities must be distributed randomly in the RVE and, second, the following condition of scale separation must be satisfied

$$d \ll l_{RVE} \ll L(\lambda) \quad (6)$$

where d is the characteristic size of the heterogeneities, l_{RVE} is the characteristic length of the RVE and L is the length of the specimen or the length of the loading (see Figure 6) (Aboudi et al., 2013; Kohlhauser & Hellmich, 2013; Zaoui, 2002). Thus, if the conditions are satisfied, the stiffness properties measured using ultrasonic tests are representative for the material. The left side of (6) ensures that the RVE is large enough to contain a sufficient number of heterogeneities and accurately depicts the composition of the material. Typically, l_{RVE} must be 2–3 times larger than d (Drugan & Willis, 1996). The right part of the inequality ensures that the RVE is small enough, such that one may consider the RVE to be subjected to virtually constant macroscopic stress and strain states, which is a requirement for *material* (rather than structural) testing. As a rule of thumb, L must be about 5–10 times larger than l_{RVE} . As for ultrasonic testing, L is equal to the wavelength λ (Kohlhauser, 2009).

Regarding the size of the specimens, 50 mm diameter was selected as this is a common diameter for ultrasonic testing of rock specimens in the literature and in the majority of cases it is sufficiently larger than the heterogeneities. The same consideration applies for the length of the specimens, where smaller lengths were not considered, as this would have a negative influence on the accuracy of detection of the arrival times. Shorter specimens and shorter travel distances result in shorter arrival times that may fall in the range of receiver disturbances (Kohlhauser & Hellmich, 2013).

Slightly different conditions are recommended by an ASTM standard that was withdrawn without replacement in 2017 and by an ISRM standard (ASTM D2845-08, 2008; Aydin, 2013). Both standards treat specifically ultrasonic testing of rock specimens. According to the ASTM standard, the length of the specimen (i.e. the flight distance) L and the lateral dimension D must fulfil the condition $L/D \leq 5$. In addition, $D \geq 5 \times \lambda_L$ (in ISRM the factor is 10). These recommendations ensure that velocities of bulk

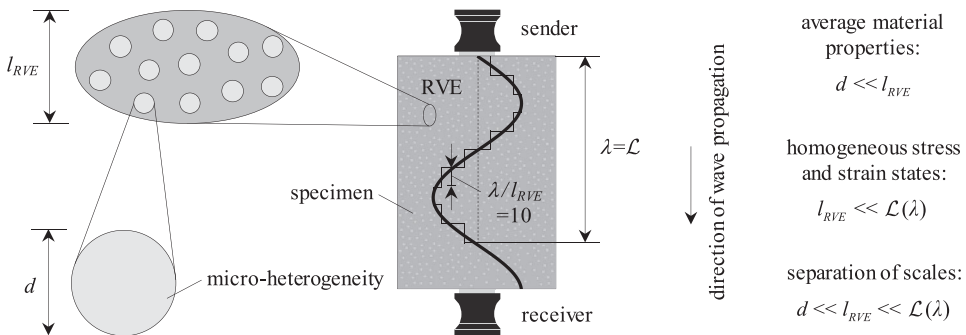


Figure 6. Scale-separation principle – the size of RVE (l_{RVE}) must be much smaller than the characteristic size of the loading in terms of wavelength (λ) for ultrasonic testing and much larger than the size of the heterogeneity (d).

waves are measured rather than velocities of bar waves. The first requirement regarding the slenderness of the specimen was also formulated by Kohlhauser and Hellmich (2013) based on comprehensive analysis of experimental results. In this study, $L/D \leq 5$ is satisfied for all specimens and $D \geq 5 \times \lambda_L$ is satisfied for all specimens at 1.00 MHz and higher frequencies. The next requirement in both the ASTM and the ISRM standard specifies that $L \geq 10 \times d$. This condition implies that three to five RVEs are included in the flight distance. The last ASTM recommendation is $\lambda_L \geq 3 \times d$.

Based on the work of Kohlhauser and Hellmich as well as the ASTM standards, the requirements for the wavelength can be systematized by introducing a dimensionless factor λ_L/d which relates the longitudinal wavelength to the grain size (microheterogeneity). Consequently, large values of λ_L/d are required in order to ensure that the material properties of the *homogenised* material are investigated. As for $\lambda_L/d < 3$ (see ASTM D2845-08, 2008), the measured pulse velocities are significantly influenced by the individual phases (microstructure). As for $\lambda_L/d > 100$ (Kohlhauser & Hellmich, 2013), the measured pulse velocities are representative for the homogenised material behaviour, even in case of an infinitely large stiffness contrast between the individual phases (e.g. aluminium specimens with air pores). Herein, we subdivide the interval of the ratio λ_L/d which ranges from 3 to 100 into two categories. They are separated by $\lambda_L/d = 20$. This value refers to a combination of $l_{RVE}/d = 2$ (Drugan & Willis, 1996) and $\lambda/l_{RVE} = 10$. The latter implies that the wavelength of ultrasonic waves is equally large as a chain of 10 RVEs. Recalling that a material test requires virtually constant stresses within the characterised material volume, $\lambda/l_{RVE} = 10$ refers to a stepwise approximation of one sine wave, using 10 equally long stress plateaus (see Figure 6). Along the described lines, we distinguish four categories defined in terms of the wavelength-over-grain size ratio λ_L/d . These categories are used to assign results of ultrasonic testing to four different levels of informative content, see Table 3.

In order to investigate the influence of the frequency on the measured velocities, five different rock specimens with different degree of heterogeneity were tested. Figure 7 shows the top view of the five specimens with their characteristic heterogeneity size d as well as the corresponding flight times of longitudinal waves with the following five frequencies: 0.05, 0.25, 1.00, 2.25, and 5.00 MHz. The heterogeneity is described by the average grain size which was assumed based on image analysis of the cross sections of the specimens. Specimens I-3A and II-5B appear quasi-homogeneous which is reflected in the smaller average grain size, whereas especially specimens I-5A and II-9B exhibit larger heterogeneities. The length and the diameter of each specimen is 50 mm.

The measured flight times together with their mean value, standard deviation, and coefficient of variation are listed in Table 4. Table 5 presents the corresponding wavelength-over-grain size ratios λ_L/d for all specimens and frequencies. The highest levels of satisfaction of the separation-of-scales principle (category 1 and 2 according to Table 3) are achieved at the lowest frequency 0.05 MHz. The same quality of the results can be expected also for specimens I-3A and II-5B at 0.25 MHz and for I-3A at 1.00 MHz. At frequencies higher than 1.00 MHz the level of satisfaction of the separation-of-scale principle is lower. Nevertheless, Figure 7 reveals no clear trend in the measured flight time associated with the change of the frequency. In fact, the standard deviation amounts to approximately 1% of the mean value, as expressed by the coefficient of variation. This is a strong indicator that different micro-heterogeneities of the tested specimens have small stiffness contrasts. The individual flight times for II-5B (kersantite) show the best consistency, while the flight times for I-3A (dolomite) reflect a slightly

Table 3. Categories based on the separation-of-scale requirement, defining levels of accuracy with which homogenised properties of materials are characterised, as a function of the ratio between wavelength (longitudinal wave) and average grain (inclusion) size, λ_L/d , as well as the stiffness contrast between individual phases.

Category	Range	Level of accuracy	Symbol
1	$\lambda_L/d \geq 100$	High accuracy even in the case of large stiffness contrast	■■■■
2	$20 \leq \lambda_L/d < 100$	High/intermediate accuracy for small/large stiffness contrast	■■■
3	$3 \leq \lambda_L/d < 20$	Intermediate/low accuracy for small/large stiffness contrast	■■
4	$\lambda_L/d < 3$	Low accuracy particularly in the case of large stiffness contrast	■

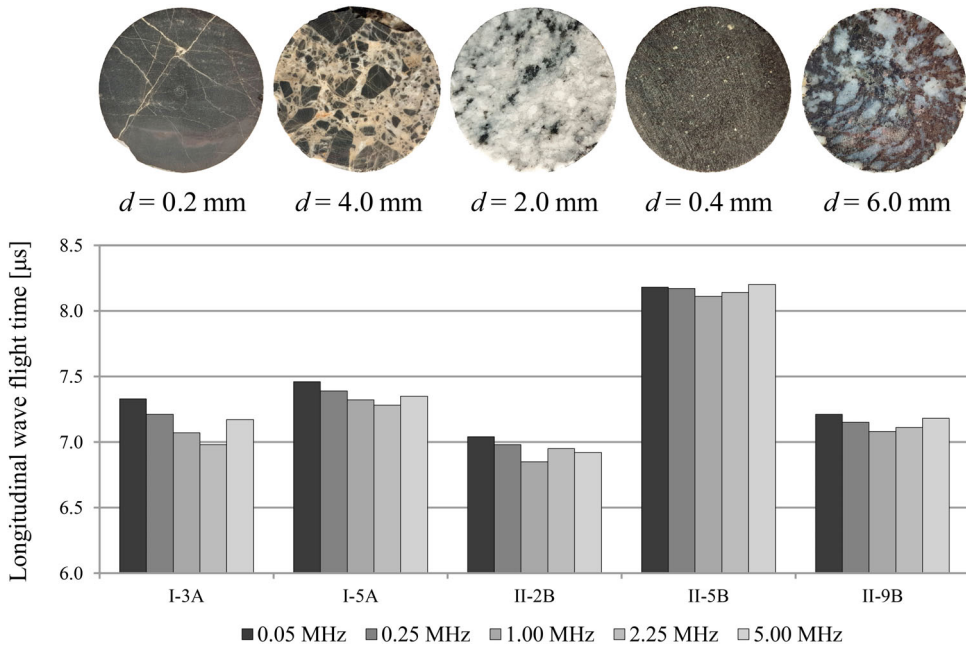


Figure 7. Variation of the measured travel time of longitudinal waves using different frequencies (from 0.05 MHz to 5.00 MHz) for two homogeneous (I-3A and II-5B) and three heterogeneous specimens (I-5A, II-2B, and II-9B).

Table 4. Flight time of longitudinal waves for five specimens depending on the frequency (from 0.05 to 5.00 MHz) with mean value, standard deviation (STDEV), and coefficient of variation (CV).

Specimen	Flight time of longitudinal waves, t_L (μs)					Mean	STDEV	CV (-)
	0.05 MHz	0.25 MHz	1.00 MHz	2.25 MHz	5.00 MHz			
I-3A	7.33	7.21	7.07	6.98	7.17	7.15	0.13	1.87%
I-5A	7.46	7.39	7.32	7.28	7.35	7.36	0.07	0.94%
II-2B	7.04	6.98	6.85	6.95	6.92	6.95	0.07	1.01%
II-5B	8.18	8.17	8.11	8.14	8.20	8.16	0.04	0.43%
II-9B	7.21	7.15	7.08	7.11	7.18	7.15	0.05	0.73%

Table 5. Ratio between wavelength (longitudinal wave) and grain size λ_L/d for five specimens depending on the frequency together with the level of fulfilment of the separation-of-scale requirement according to the categories of Table 3.

Specimen	Ratio of wavelength to grain size (longitudinal waves), λ_L/d (-)					Average d (mm)
	0.05 MHz	0.25 MHz	1.00 MHz	2.25 MHz	5.00 MHz	
I-3A	684.2	27.8	35.5	16.0	7.0	0.2
I-5A	32.7	6.6	1.7	0.7	0.3	4.0
II-2B	70.9	14.3	3.6	1.6	0.7	2.0
II-5B	306.0	61.3	15.4	6.8	3.1	0.4
II-9B	23.1	4.7	1.2	0.5	0.2	6.0

larger variation. In summary, there is no (linear) dependence between the measured flight times and the ultrasonic frequency or the size of the heterogeneities. However, it must be noted that the RVEs characterised with 0.05 MHz are not well separated by scale from the specimen length.

A similar analysis using transversal waves had to be limited to 2.25 and 5.00 MHz, because only at these frequencies it was possible to accurately determine the arrival times of transversal waves. In this context, it is noteworthy that transversal waves are less sensitive to microheterogeneities in the

material, as compared to longitudinal waves (see Kohlhauser, 2009). Anyway, 2.25 MHz is the lowest frequency that allowed for reliable identification of arrival times of both longitudinal and transversal waves. Notably, ultrasonic tests with 2.25 MHz fall into the λ_L/d -categories 3 and 4. Still, the rather small stiffness contrasts within the different constituents of the tested rock specimens, going along with ultrasonic results that are virtually constant across all four λ_L/d -categories, suggest that the results obtained with 2.25 MHz are of satisfactory quality for engineering purposes, where an accuracy of $\pm 2\%$ is sufficient. Thus, while the influence of the individual phases (microstructure) is expected to be more pronounced at higher frequencies (lower wavelengths), in this case the effect might be mitigated by lower stiffness contrast between the individual phases.

4.3. Results and discussion

The main results of this study for all specimens from quarry I and quarry II are presented in Tables 6 and 7, respectively. All measurements were conducted at room temperature, because the influence of temperature on the elastic properties is expected to be negligible for dry specimens and temperatures below 40°C, for which asphalt mixtures are typically tested (Schön, 2015). Three specimens from quarry I (marked with asterisk) were excluded from further analysis due to excessive cracking. The measured ultrasonic velocities range from 5.6 to 7.3 km/s for the longitudinal wave and from 3.1 to 4.0 km/s for the transversal wave. For the majority of the specimens, Poisson's ratios between 0.20 and 0.30 were computed. Figure 8 gives an overview of the calculated shear, bulk, and elastic moduli grouped according to rock type, quarry, and specimen length with the number of specimens in each group given at the bottom of the figure. The box plots provide the minimum, the 25th percentile, the median, the 75th percentile, the maximum, and the mean value of the moduli in a specific group.

The first six box plots from left to right illustrate the results for the different rocks types. First, it can be observed that the limestone from quarry I has a lower stiffness than the dolomite samples from the same source. There are no large differences between I-1 to I-4 (quasi-homogeneous) and I-5, I-6 (two-phase composite), despite the different texture and the potentially different mineral composition. The fine-grained rock kersantite (II-5 and II-6) has the lowest variation in stiffness properties from

Table 6. Test results for all specimen from quarry I including length, diameter, dry density, shear modulus, bulk modulus, Poisson ratio, and elastic modulus based on travel time measurements using longitudinal and transversal ultrasonic waves.

Specimen	Length, L (mm)	Diameter, D (mm)	Mass Density, ρ (kg/m ³)	Shear modulus, G (GPa)	Bulk modulus, K (GPa)	Possion's ratio, ν (-)	Elastic modulus, E (GPa)	Comment
I-1A	49	55	2825	44	93	0.30	113	
I-2A	50	50	2825	43	90	0.29	111	
I-2B	50	50	2826	43	90	0.30	110	
I-2C	100	50	2824	40	83	0.29	104	
I-3A	50	50	2815	42	89	0.30	109	
I-3B	50	50	2749	34	64	0.27	88	
I-3C	100	50	2804	28	85	0.35	75	*damaged
I-4A	50	50	2797	38	82	0.30	98	
I-4B	50	50	2800	39	85	0.30	103	
I-5A	49	50	2784	37	75	0.29	96	
I-6A	50	50	2793	39	88	0.31	101	
I-6B	50	50	2781	39	82	0.29	102	
I-7A	50	50	2721	36	75	0.29	94	
I-7B	50	50	2734	32	69	0.30	83	
I-8A	50	50	2655	28	67	0.31	75	
I-8B	50	50	2653	29	68	0.32	75	
I-8C	99	50	2662	30	65	0.30	78	
I-9A	50	50	2742	36	74	0.29	92	
I-9B	50	50	2641	30	60	0.28	77	
I-9C	100	50	2492	14	42	0.35	38	*cracked
I-9D	100	50	2554	24	51	0.30	62	*damaged

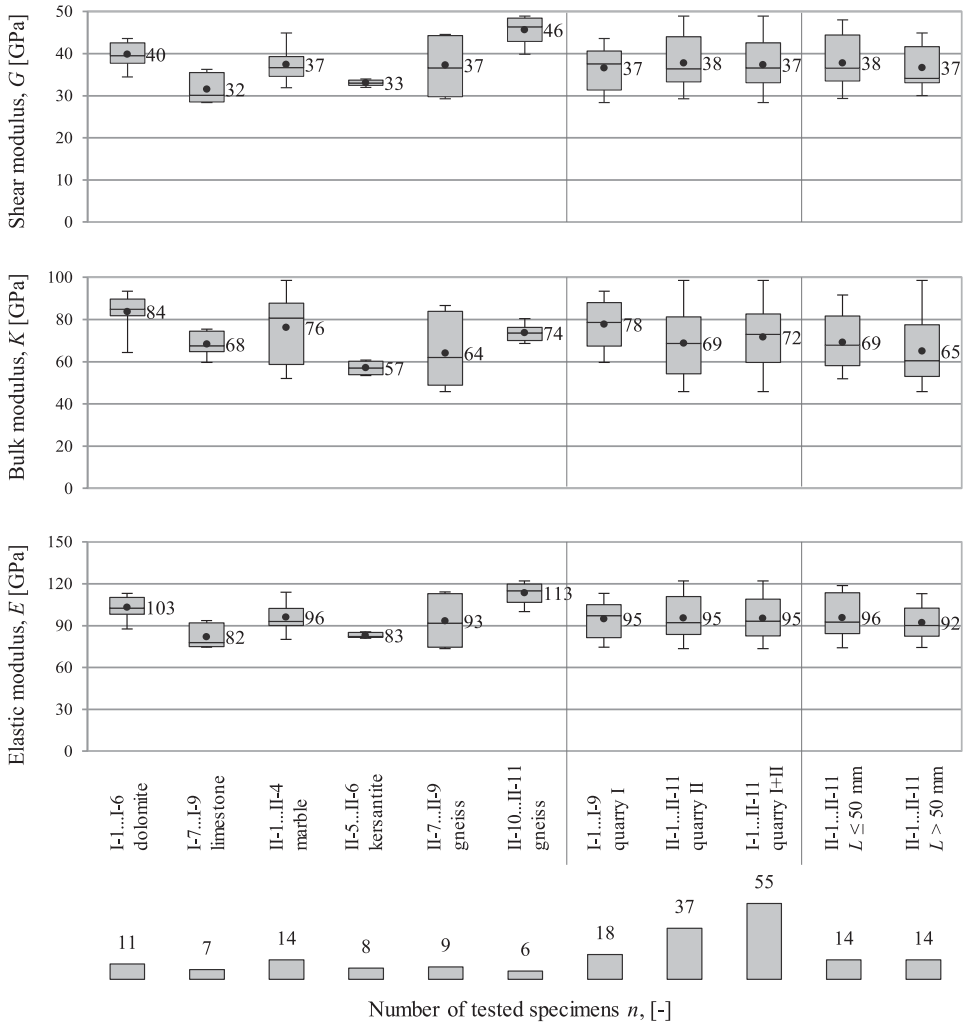


Figure 8. Box-plot summary of test results for shear, bulk, and elastic modulus. Comparison of six different rock types, two different sources (quarries) and influence of specimen length with number of tested specimens in each group.

all rock types, also having the most homogeneous appearance. The stiffness of kersantite is found to be comparable with the stiffness of limestone, with the latter even possessing higher bulk modulus. The largest variation is attributed to the first gneiss group (II-7 to II-9). Table 7 reveals that the variation between samples from the same stone is very small for all rock types including gneiss. Thus, it can be seen that the variation in the group II-7 to II-9 is caused by variation between the stiffness of the individual stones (from 74 to 114 GPa). Furthermore, the second gneiss group (II-10 and II-11) achieved the highest stiffness values with regard to shear modulus and elastic modulus, while the highest bulk modulus values were recorded for dolomite (I-1 to I-6).

One explanation of the variation in the first gneiss group lies in the possibly different qualitative and quantitative mineral composition which was determined only for sample II-7 (see Section 3.2). Even if the composition of two samples is similar, the difference in the stiffness may be caused by anisotropy effects due to preferred mineral orientation, mineral layering, and anisotropic cracks. In the literature, it has been shown that the ultrasonic velocity parallel to an anisotropy plane (e.g. parallel to gneiss banding) can be significantly higher than the velocity perpendicular to the anisotropy plane (e.g. Ivankina

Table 7. Test results for all specimen from quarry II including length, diameter, dry density, shear modulus, bulk modulus, Poisson ratio, and elastic modulus based on travel time measurements using longitudinal and transversal ultrasonic waves.

Specimen	Length, L (mm)	Diameter, D (mm)	Mass Density, ρ (kg/m^3)	Shear modulus, G (GPa)	Bulk modulus, K (GPa)	Possion's ratio, ν (-)	Elastic modulus, E (GPa)	Comment
II-1A	50	50	2845	37	73	0.28	95	
II-1B	50	50	2852	37	59	0.24	93	
II-1C	99	50	2841	37	52	0.21	90	
II-1D	150	50	2850	32	54	0.25	80	cracks
II-1E	150	50	2845	34	56	0.25	86	cracks
II-2A	50	50	2839	45	82	0.27	114	
II-2B	50	50	2845	44	88	0.28	114	
II-2C	99	50	2846	43	83	0.28	110	
II-3A	50	50	2777	38	88	0.31	100	
II-3B	50	50	2724	36	95	0.33	97	
II-3C	100	50	2799	34	98	0.35	90	
II-4A	42	50	2712	35	81	0.31	92	
II-4B	49	50	2713	36	81	0.31	93	
II-4C	100	50	2735	35	76	0.30	90	
II-5A	50	50	2778	34	60	0.26	85	
II-5B	50	50	2774	34	60	0.26	86	
II-5C	100	50	2781	32	60	0.27	82	
II-5D	150	50	2793	33	61	0.27	85	
II-6A	50	50	2614	32	54	0.25	81	
II-6B	47	50	2611	33	54	0.25	82	Figure 5
II-6C	84	50	2632	33	54	0.25	82	
II-6D	100	50	2619	33	53	0.24	82	
II-7A	50	50	2946	37	62	0.25	92	
II-7B	46	50	2975	36	64	0.26	90	
II-7C	84	50	2939	41	46	0.15	95	
II-8A	50	50	2769	29	53	0.27	75	
II-8B	50	50	2755	29	51	0.26	74	
II-8C	100	50	2754	30	47	0.24	74	
II-9A	50	50	2896	45	87	0.28	114	
II-9B	50	50	2902	44	85	0.28	113	
II-9C	96	50	2913	44	83	0.27	113	
II-10A	48	50	2962	44	71	0.24	109	
II-10B	47	50	3025	49	80	0.25	122	
II-10C	100	50	2948	40	69	0.26	100	
II-11A	50	50	2988	48	75	0.24	118	
II-11B	50	50	2997	48	74	0.23	119	
II-11C	100	50	3002	45	73	0.24	112	

et al., 2017; Park & Min, 2015; Schön, 2015; Song et al., 2004). Possible anisotropy effects cannot be deduced by comparison of samples from the same stone because the specimens were almost always drilled in the same direction (parallel to each other). From this point of view, the production of cube specimens would have been an interesting choice, allowing for investigation of stiffness properties in three directions. Similarly, the specimens from stone II-2 exhibited higher values for elastic modulus compared to the other stones from the dolomitic marble group. In the literature, mineral aggregates are assumed to be isotropic as a simplification and due to their random orientation in the asphalt mixtures (Wang, 2011). Nevertheless, the assumption about the random orientation is also questionable as compaction methods have influence on the orientation of coarse aggregates (Little et al., 2018). Apart from that, the results also show that potential anisotropic effects appear to be rather small, at least for specific aggregates (e.g. dolomite, kersantite).

Furthermore, the comparison between quarry I and quarry II reveals that the variation in quarry II is slightly larger, which is normal considering the larger number of specimens and different rock types. Notably, the mean values of the elastic moduli for both quarries are the same, equalling 95 GPa. The last two box plots compare specimens with 50 mm and specimens with 100/150 mm length ($L > 50$ mm). If a specific stone is represented by two specimens with $L = 50$ and one specimen with $L > 50$ mm,

the values of the first two specimens are replaced by their mean. This procedure enables the comparability of the two groups which now include equal number of specimens. The comparison shows a slight reduction of the stiffness values with increasing length of the specimens. However, as Table 7 shows, this conclusion is rock type-specific as specimens II-5 to II-9 (kersantite and gneiss) exhibit a virtually constant stiffness. This is characteristic of homogeneous elastic materials, whose stiffness properties are independent of the specimen length, as long as specific minimum dimensions and ratio recommendations for the sample geometry are met (Kohlhauser & Hellmich, 2013). The slight decrease of stiffness for other two rock types can be explained by slightly different mineral composition or orientation, variation due to measurement accuracy, or small non-uniform inhomogeneities (defects, cracks) which are more likely to occur with increasing length of the specimen. This comparison applies only to quarry II, as only two specimens with length above 50 mm were extracted from the samples of the first quarry.

Apart from these slight deviations, the results suggest that pores and other inhomogeneities are distributed randomly across the specimen volume. As regards the influence of porosity on the stiffness values, porosity plays the role of a microstructural constituent. Provided that the size of the pores is significantly smaller than the wavelength of the ultrasonic waves, the speed of elastic ultrasonic waves is representative for the porous material. This implies that porosity is accounted for in the macroscopic stiffnesses communicated in Tables 6 and 7.

5. Significance for multi-scale modelling of asphalt

The main goal of this study is to investigate the elastic properties of mineral aggregates from specific sources which can be used as an input for multi-scale models of asphalt mixtures. Figure 9 illustrates a multi-scale model considering five different scales (Eberhardsteiner et al., 2015a; Lackner et al., 2004; Pichler et al., 2012), although there are also models that consider the microstructure of the binder (Eberhardsteiner et al., 2015b). In the presented model, mineral aggregates participate as a material phase at three different scales, namely at the mastic, mortar, and mixture scale as filler, fine aggregates, and coarse aggregates, respectively.

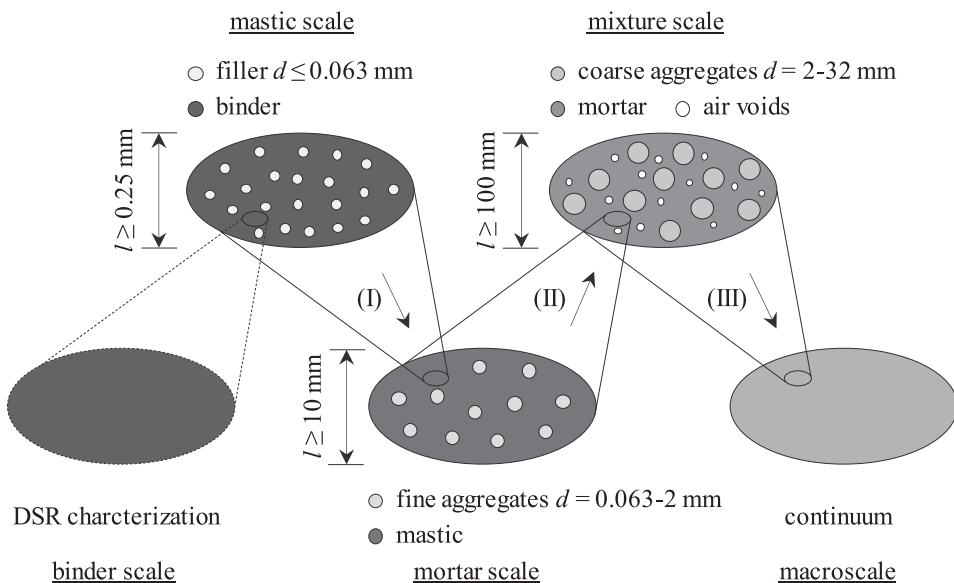


Figure 9. Multi-scale model for asphalt concrete mixtures with two-dimensional representation of three-dimensional RVEs and mineral aggregate properties being used as input on three levels of observation: mastic, mortar, and mixture.

5.1. Appropriateness of test method

In the literature on rock testing, uniaxial compression tests (UCT), triaxial compression tests, seismic velocity measurements, ultrasonic tests, and nanoindentation are used for determination of the elastic properties. The most common test methods are uniaxial compression tests and ultrasonic tests on cylindrical specimens. Many studies have been conducted on comparing the results of both types of tests (often referred to as static and dynamic test, respectively), deriving correlation equations and explaining the sources for differences (e.g. Brotons et al., 2016; Christaras et al., 1994; Ciccotti & Mulargia, 2004; Davarpanah et al., 2020; Fjær, 2019; Heerden, 1987; Kibikas et al., 2020; Martinez-Martinez et al., 2012; Moradian & Behnia, 2009). Irfan-ul-Hassan et al. (2016) have shown that the modulus of elasticity obtained from evaluating quasi-static tests based on the linear theory of viscoelasticity is practically the same as the modulus of elasticity obtained by ultrasonic tests for cement paste specimens. For natural, less homogeneous materials like rocks, the modulus obtained by quasi-static tests might be lower than the ultrasonic modulus. One possible explanation for this phenomenon is the occurrence of inelastic deformation during quasi-static tests caused by sliding cracks and grain boundaries. Because inelastic waves are slower than elastic waves, and because of the very small stress amplitudes of ultrasonic stress waves, ultrasonic testing is very robust with respect to possible inelastic processes. Furthermore, the stresses and strains induced by ultrasonic testing are much lower than the typical stresses and strains in quasi-static testing (Schön, 2015). Hence, it is assumed that the results from ultrasonic tests are more representative of the pure elastic properties.

Beyond that, ultrasonic testing offers several advantages in comparison to UCT and nanoindentation. First, there is not even a slight risk of damaging the specimen and the only source of errors (besides systematic errors) is the determination of the arrival time of the wave. Second, the evaluation of the results is straight-forward, with no additional models or assumptions being necessary. The main testing parameter that has to be selected is the wave frequency. Ultrasonic tests are easy to conduct with a test duration of just a few minutes.

In comparison, for UCT the following parameters have to be determined: maximum stress limit, minimum stress limit, loading rate, number of loading and unloading cycles, measurement length. There are also many approaches for calculation of the modulus obtained by quasi-static tests: based on loading path, on the unloading path, specific range of the loading/unloading path, secant or tangent modulus at a specific stress level. UCT requires more specimens, more time and effort and the determination of Poisson's ratio is cumbersome. Furthermore, shear stresses due to friction in the interface steel platen/specimen may lead to inhomogeneous stress distribution over a length equal to the diameter of the specimen. Hence, the ratio L/D must be larger or at least equal to 3 and the strains must be measured over the central region of the specimen with measurement length $L - 2 \times D$ (Karte et al., 2015).

Nanoindentation is also a very time- and effort-consuming method requiring a large number of indentations for reliable statistical analysis. Similarly, to UCT, the evaluation and interpretation of the results is a challenging task. Moreover, Poisson's ratio cannot be measured and has to be assumed.

5.2. Material characterisation scale

According to the European standard EN 13043 (2002), mineral aggregates in asphalt mixtures can be divided into filler aggregates with particle size under 0.0063 mm, fine aggregates (sand) with particle size between 0.0063 and 2 mm, and coarse aggregate with particle size between 2 and 32 mm. As the multi-scale model in Figure 9 employs the same classification, a characterisation of the aggregates over these three length scales is necessary. It is possible that all three categories of aggregate originate from the same source and belong to the same rock type. However, often added filler (produced separately), aggregates from multiple sources and recycling material are used in asphalt mixtures which would make the exact determination of the mechanical properties of aggregates difficult. With the conducted ultrasonic tests, the material properties of rock specimens were determined at the scale

from 0.3 to 0.6 mm, which is estimated as one fifth and one tenth of an average wavelength of 3.0 mm for 2.25 MHz frequency. However, Section 4.2. suggests that the validity of the results can be extended at least to the range from 0.14 mm ($\lambda_{5\text{MHz}}$) to 26 mm ($\lambda_{0.05\text{MHz}}$), which covers the length scale of fine and coarse aggregates. In contrast, the uniaxial compression tests characterise the material volume between the linear variable differential transducers (LVDTs) which is normally much larger than 26 mm (e.g. 100 mm). Thus, UCT and ultrasonic tests probe different rock volumes and the material characterisation scale provided by ultrasonic testing is more adequate considering the size of mineral aggregates in asphalt mixtures.

As concerns the elastic properties of the filler, the filler particles are so small that (i) one may assume that they consist of single crystals rather than representing minerals (i.e. composites of different crystals), and (ii) it is unlikely that they contain significant defects or cracks. Thus, one may assign single-crystal stiffness properties to the filler particles using values from the literature (e.g. Simmons & Wang, 1971) or other experiments (e.g. nanoindentation). The stiffness of a single filler particle depends, because of anisotropy, on the crystal orientation. The entire filler phase may contain particles of different crystals according to the mineralogical composition of the rocks used to produce the filler. Due to the random orientation of mineralogically different anisotropic filler particles in the mastic, an effective average isotropic elastic stiffness can be assigned to the (entire) filler phase.

Alternatively, DSR experiments can be used to characterise the mechanical properties of the binder and of the bitumen-filler composite (mastic). Thus, by applying the multi-scale model to estimate the stiffness properties of the mastic (i.e. the first homogenisation step), the average elastic isotropic properties of the entire filler phase can be back-calculated.

6. Conclusions

The elastic properties of mineral aggregates in asphalt mixtures are rarely being investigated, as they are not currently considered in pavement and mix design standards and tools. However, the determination of these properties is of interest, as they constitute an important input to (multi-scale) micromechanical models used for upscaling-based prediction of the mechanical properties of composite asphalt materials, particularly at low temperatures and high frequencies.

In this study, the elastic stiffness properties of rock materials used in asphalt mixtures were characterised. For this purpose, a total of 55 cylindrical specimens from two different quarries were produced and tested using the ultrasonic through transmission technique. X-ray powder diffractometry revealed that the main rock types are dolomite, limestone, dolomitic marble, kersantite, and gneiss. It was observed that measured flight times and velocities for longitudinal waves showed only a very small variation in the interval of wave frequencies ranging from 0.05 MHz to 5.00 MHz. Still, the results show a significant variation in the measured stiffness characteristics between the different types of rock and low variation between different samples from the same stone. Limestone and kersantite exhibited the lowest values of the elastic modulus: 82 and 83 GPa, respectively. The elastic properties of kersantite showed a very low variation between samples regardless of the sample length. Other type of rocks like dolomite marble and dolomite achieved a higher elastic modulus of 96 and 103 GPa, respectively. The largest elastic modulus of 113 GPa was measured for the rock type biotite-amphibole-garnet-gneiss. In addition, the average stiffness properties of the aggregates from both quarries are quite similar. As regards input for micromechanical models, it is noteworthy that the shear modulus averaged over all 55 rock specimens is equal to 37 GPa, and the corresponding average bulk modulus amounts to 72 GPa, both being considerably larger than typical values used for upscaling of the stiffness of asphalt mixtures.

For the application of multi-scale models to asphalt mixtures containing different aggregate materials (i.e. different rock type or quarry source), it is recommended to quantify the stiffness of the aggregates by applying the here-described protocol. The stiffness of the aggregates from

the same quarry has to be examined de novo only if substantial changes in the material composition and quality are observed. The mechanical properties of the binder, in turn, have to be investigated every time for each asphalt mixture, as they depend on both the source and the batch.

Acknowledgment

The authors thank Karin Wriessnig and Franz Ottner (Institute for Applied Geology of the University of Natural Resources and Applied Life Sciences, Austria) for conducting the X-ray powder diffraction analysis and the classification of the rocks, David Valentin for the preparation of the specimens and Luis Zelaya-Lainez for the interesting discussions.

Disclosure statement

No potential conflict of interest was reported by the author(s).

Funding

The authors also acknowledge the TU Wien University Library for financial support through its Open Access Funding Programme.

ORCID

Valentin Donev  <http://orcid.org/0000-0002-3933-971X>

Olaf Lahayne  <http://orcid.org/0000-0002-5252-1356>

Bernhard Pichler  <http://orcid.org/0000-0002-6468-1840>

Lukas Eberhardsteiner  <http://orcid.org/0000-0003-2153-9315>

References

- AASHTO. (2015). *Mechanistic-empirical pavement design guide: A manual of practice* (2nd ed.). American Association of State Highway and Transportation Officials.
- AASHTO T 315. (2013). *Determining the rheological properties of asphalt binder using a dynamic shear rheometer (DSR)*. American Association of State Highway and Transportation Officials.
- Aboudi, J., Arnold, S. M., & Bednarczyk, B. A. (2013). *Micromechanics of composite materials: A generalized multiscale analysis approach*. Elsevier.
- Allen, D. H., Little, D. N., Soares, R. F., & Berthelot, C. (2017). Multi-scale computational model for design of flexible pavement – part I: Expanding multi-scaling. *International Journal of Pavement Engineering*, 18(4), 309–320. <https://doi.org/10.1080/10298436.2015.1065999>
- Allmann, R. (2003). *Röntgenpulverdiffraktometrie: Rechnergestützte Auswertung, Phasenanalyse und Strukturbestimmung* [X-ray powder diffraction: Computer-assisted evaluation, phase identification and structure determination]. Springer (in German).
- Arshadi, A., & Bahia, H. (2015). Development of an image-based multiscale finite-element approach to predict mechanical response of asphalt mixtures. *Road Materials and Pavement Design*, 16(sup2), 214–229. <https://doi.org/10.1080/14680629.2015.1077007>
- ASTM D2845-08. (2008). *Standard test method for laboratory determination of pulse velocities and ultrasonic elastic constants of rock (withdrawn 2017)*. ASTM International.
- Aydin, A. (2013). Upgraded ISRM suggested method for determining sound velocity by ultrasonic pulse transmission technique. In R. Ulusay (Ed.), *The ISRM suggested methods for rock characterization, testing and monitoring: 2007–2014* (pp. 95–99). Springer. https://doi.org/10.1007/978-3-319-07713-0_6
- Barbhuiya, S., & Caracciolo, B. (2017). Characterisation of asphalt concrete using nanoindentation. *Materials*, 10(7), <https://doi.org/10.3390/ma10070823>
- Bari, J., & Witczak, M. (2006). Development of a new revised version of the Witczak E* predictive model for hot mix asphalt mixtures (with discussion). *Journal of the Association of Asphalt Paving Technologists*, 75, 381–423.
- Brotons, V., Tomas, R., Ivorra, S., Grediaga, A., Martinez-Martinez, J., Benavente, D., & Gomez-Heras, M. (2016). Improved correlation between the static and dynamic elastic modulus of different types of rocks. *Materials and Structures*, 49(8), 3021–3037. <https://doi.org/10.1617/s11527-015-0702-7>
- Carcione, J. M. (2014). *Wave fields in real media: Wave propagation in anisotropic, anelastic, porous and electromagnetic media* (3rd ed.). Elsevier.

- Ceylan, H., Gopalakrishnan, K., & Kim, S. (2009). Looking to the future: The next-generation hot mix asphalt dynamic modulus prediction models. *International Journal of Pavement Engineering*, 10(5), 341–352. <https://doi.org/10.1080/10298430802342690>
- Charitaras, B., Auger, F., & Mosse, E. (1994). Determination of the moduli of elasticity of rocks. Comparison of the ultrasonic velocity and mechanical resonance frequency methods with direct static methods. *Materials and Structures*, 27(4), 222–228. <https://doi.org/10.1007/BF02473036>
- Christensen, D. W., & Bonaquist, R. (2015). Improved Hirsch model for estimating the modulus of hot-mix asphalt. *Road Materials and Pavement Design*, 16(sup2), 254–274. <https://doi.org/10.1080/14680629.2015.1077635>
- Ciccotti, M., & Mulargia, F. (2004). Differences between static and dynamic elastic moduli of a typical seismogenic rock. *Geophysical Journal International*, 157(1), 474–477. <https://doi.org/10.1111/j.1365-246X.2004.02213.x>
- Clearfield, A., Reibenspies, J. H., & Bhuvanesh, N. (Eds.). (2008). *Principles and applications of powder diffraction*. Wiley.
- Coleri, E., Harvey, J. T., Yang, K., & Boone, J. M. (2012). Development of a micromechanical finite element model from computed tomography images for shear modulus simulation of asphalt mixtures. *Construction and Building Materials*, 30, 783–793. <https://doi.org/10.1016/j.conbuildmat.2011.12.071>
- Davarpanah, S. M., Ván, P., & Vászárhelyi, B. (2020). Investigation of the relationship between dynamic and static deformation moduli of rocks. *Geomechanics and Geophysics for Geo-Energy and Geo-Resources*, 6(1), <https://doi.org/10.1007/s40948-020-00155-z>
- Drugan, W., & Willis, J. (1996). A micromechanics-based nonlocal constitutive equation and estimates of representative volume element size for elastic composites. *Journal of the Mechanics and Physics of Solids*, 44(4), 497–524. [https://doi.org/10.1016/0022-5096\(96\)00007-5](https://doi.org/10.1016/0022-5096(96)00007-5)
- Eberhardsteiner, L., & Blab, R. (2017). Design of bituminous pavements – a performance-related approach. *Road Materials and Pavement Design*, 20(2), 244–258. <https://doi.org/10.1080/14680629.2017.1380689>
- Eberhardsteiner, L., Füssl, J., Hofko, B., & Blab, R. (2015a). Prediction of hot mix asphalt stiffness – a multiscale approach. In: *TRB 94th Annual Meeting Compendium of Papers*.
- Eberhardsteiner, L., Füssl, J., Hofko, B., Handle, F., Hospodka, M., Blab, R., & Grothe, H. (2015b). Influence of asphaltene content on mechanical bitumen behavior: Experimental investigation and micromechanical modeling. *Materials and Structures*, 48(10), 3099–3112. <https://doi.org/10.1617/s11527-014-0383-7>
- El-Badawy, S., Abd El-Hakim, R., & Awed, A. (2018). Comparing artificial neural networks with regression models for hot-mix asphalt dynamic modulus prediction. *Journal of Materials in Civil Engineering*, 30(7), 04018128. [https://doi.org/10.1061/\(ASCE\)MT.1943-5533.0002282](https://doi.org/10.1061/(ASCE)MT.1943-5533.0002282)
- EN 13043. (2002). *Aggregates for bituminous mixtures and surface treatments for roads, airfields and other trafficked areas*. European Committee for Standardization (CEN).
- EN 14770. (2012). *Bitumen and bituminous binders – Determination of complex shear modulus and phase angle using a dynamic shear rheometer (DSR)*. European Committee for Standardization (CEN).
- Ermich, M., & Oppen, D. (2013). *X-ray powder diffraction – XRD for the analyst: Getting acquainted with the principles*. PANalytical B.V.
- Fakhari Tehrani, F., Absi, J., Allou, F., & Petit, C. (2018). Micromechanical modelling of bituminous materials' complex modulus at different length scales. *International Journal of Pavement Engineering*, 19(8), 685–696. <https://doi.org/10.1080/10298436.2016.1199879>
- Fjær, E. (2019). Relations between static and dynamic moduli of sedimentary rocks. *Geophysical Prospecting*, 67(1), 128–139. <https://doi.org/10.1111/1365-2478.12711>
- Golafshani, E. M., & Behnoud, A. (2018). Automatic regression methods for formulation of elastic modulus of recycled aggregate concrete. *Applied Soft Computing*, 64, 377–400. <https://doi.org/10.1016/j.asoc.2017.12.030>
- Gong, H., Sun, Y., Dong, Y., Hu, W., Han, B., Polaczyk, P., & Huang, B. (2021). An efficient and robust method for predicting asphalt concrete dynamic modulus. *International Journal of Pavement Engineering*. Advance online publication. <https://doi.org/10.1080/10298436.2020.1865533>
- Heerden, W. L. (1987). General relations between static and dynamic moduli of rocks. *International Journal of Rock Mechanics and Mining Sciences & Geomechanics Abstracts*, 24(6), 381–385. [https://doi.org/10.1016/0148-9062\(87\)92262-5](https://doi.org/10.1016/0148-9062(87)92262-5)
- Hernandez, J., Sawalha, M., Rivera-Perez, J., Ozer, H., & Al-Qadi, I. L. (2018). Micromechanical modeling of I-FIT asphalt concrete specimens. *Engineering Fracture Mechanics*, 200, 234–250. <https://doi.org/10.1016/j.engfracmech.2018.07.033>
- Hofko, B., Kirchmaier, L., & Blab, R. (2011). *Assessment of the polishing behavior of sand using the test device according to Wehner/Schulze*. Proceedings of the 5th International Conference on Bituminous Mixtures and Pavements. Thessaloniki, Greece.
- Irfan-ul-Hassan, M., Pichler, B., Reihnsner, R., & Hellmich, C. (2016). Elastic and creep properties of young cement paste, as determined from hourly repeated minute-long quasi-static tests. *Cement and Concrete Research*, 82, 36–49. <https://doi.org/10.1016/j.cemconres.2015.11.007>
- Ivankina, T. I., Zel, I. Y., Lokajicek, T., Kernd, H., Lobanov, K. V., & Zharikov, A. V. (2017). Elastic anisotropy of layered rocks: Ultrasonic measurements of plagioclase-biotite-muscovite (sillimanite) gneiss versus texture-based theoretical predictions (effective media modeling). *Tectonophysics*, 712-713, 82–94. <https://doi.org/10.1016/j.tecto.2017.05.005>
- Karki, P., Kim, Y.-R., & Little, D. N. (2015). Dynamic modulus prediction of asphalt concrete mixtures through computational micromechanics. *Transportation Research Record*, 2507(1), 1–9. <https://doi.org/10.3141/2507-01>

- Karte, P., Hlobil, M., Reihnsner, R., Dörner, W., Lahayne, O., Eberhardsteiner, J., & Pichler, B. (2015). Unloading-based stiffness characterisation of cement pastes during the second, third and fourth day after production. *Strain*, 51(2), 156–169. <https://doi.org/10.1111/str.12129>
- Khan, Z. H., Tarefder, R. A., & Faisal, H. M. (2021). Multiscale modeling of asphalt concrete and validation through instrumented pavement section. *Transportation Research Record*, 2675(6), 117–136. <https://doi.org/10.1177/0361198121989723>
- Kibikas, W. M., Carpenter, B. M., & Ghassemi, A. (2020). Mechanical strength and physical properties of Oklahoma's igneous basement. *Tectonophysics*, 777, 228336. <https://doi.org/10.1016/j.tecto.2020.228336>
- Kim, M., & Buttlar, W. G. (2010). Stiffening mechanisms of asphalt–aggregate mixtures: From binder to mixture. *Transportation Research Record*, 2181(1), 98–108. <https://doi.org/10.3141/2181-11>
- Kohlhauser, C. (2009). *Elasticity tensor determination by means of ultrasonic pulse transmission: application ranges in terms of specimen geometry and microstructure, off-diagonal tensor components, as well as different engineering and biomedical materials* [Doctoral dissertation, TU Wien]. repositUM. <https://repositum.tuwien.at/handle/20.500.12708/12960>
- Kohlhauser, C., & Hellmich, C. (2013). Ultrasonic contact pulse transmission for elastic wave velocity and stiffness determination: Influence of specimen geometry and porosity. *Engineering Structures*, 47, 115–133. <https://doi.org/10.1016/j.engstruct.2012.10.027>
- Kollmann, J., Liu, P., Lu, G., Wang, D., Oeser, M., & Leischner, S. (2019). Investigation of the microstructural fracture behaviour of asphalt mixtures using the finite element method. *Construction and Building Materials*, 227. <https://doi.org/10.1016/j.conbuildmat.2019.117078>
- Krautkrämer, J., & Krautkrämer, H. (1990). *Ultrasonic testing of materials* (4th ed.). Springer. <https://doi.org/10.1007/978-3-662-10680-8>
- Lackner, R., Blab, R., Jäger, A., Spiegel, M., Kappl, K., Wistuba, M., Gagliano, B., & Eberhardsteiner, J. (2004). Multiscale modeling as the basis for reliable predictions of the behaviour of multi-composed materials. In B. H. V. Topping, & C. A. Mota Soares (Eds.), *Progress in engineering computational technology* (pp. 153–188). Saxe-Coburg Publications. <https://doi.org/10.4203/csets.12.8>
- Little, D. N., Allen, D. H., & Bhasin, A. (2018). *Modeling and design of flexible pavements and materials*. Springer.
- Martinez-Martinez, J., Benavente, D., & Garcia-del-Cura, M. A. (2012). Comparison of the static and dynamic elastic modulus in carbonate rocks. *Bulletin of Engineering Geology and the Environment*, 71(2), 263–268. <https://doi.org/10.1007/s10064-011-0399-y>
- Moradian, Z. A., & Behnia, M. (2009). Predicting the uniaxial compressive strength and static Young's modulus of intact sedimentary rocks using the ultrasonic test. *International Journal of Geomechanics*, 9(1), 14–19. [https://doi.org/10.1061/\(ASCE\)1532-3641\(2009\)9:1\(14\)](https://doi.org/10.1061/(ASCE)1532-3641(2009)9:1(14))
- Nikolaides, A. (2015). *Highway engineering: Pavements, materials and control of quality*. CRC Press.
- Park, B., & Min, K.-B. (2015). Bonded-particle discrete element modeling of mechanical behavior of transversely isotropic rock. *International Journal of Rock Mechanics and Mining Sciences*, 76, 243–255. <https://doi.org/10.1016/j.ijrmps.2015.03.014>
- Pecharsky, V. K., & Zavalij, P. Y. (2009). *Fundamentals of powder diffraction and structural characterization of materials* (2nd ed.). Springer.
- Pichler, C., Lackner, R., & Aigner, E. (2012). Generalized self-consistent scheme for upscaling of viscoelastic properties of highly-filled matrix-inclusion composites – Application in the context of multiscale modeling of bituminous mixtures. *Composites Part B: Engineering*, 43(2), 457–464. <https://doi.org/10.1016/j.compositesb.2011.05.034>
- Sakhaeifar, M. S., Underwood, B. S., Kim, Y. R., Puccinelli, J., & Jackson, N. (2010). Development of artificial neural network predictive models for populating dynamic moduli of long-term pavement performance sections. *Transportation Research Record*, 2181(1), 88–97. <https://doi.org/10.3141/2181-10>
- Sawda, C. E., Fakhari-Tehrani, F., Absi, J., Allou, F., & Petit, C. (2019). Multiscale heterogeneous numerical simulation of asphalt mixture. *Material Design & Processing Communications*, 1(3), 3. <https://doi.org/10.1002/mdp2.42>
- Schön, J. (2015). *Physical properties of rocks: Fundamentals and principles of petrophysics* (2nd ed.). Elsevier.
- Simmons, G., & Wang, H. (1971). *Single crystal elastic constants and calculated aggregate properties: A handbook* (2nd ed.). The MIT Press.
- Singh, D., Zaman, M., & Commuri, S. (2013). Artificial neural network modeling for dynamic modulus of hot mix asphalt using aggregate shape properties. *Journal of Materials in Civil Engineering*, 25(1), 54–62. [https://doi.org/10.1061/\(ASCE\)MT.1943-5533.0000548](https://doi.org/10.1061/(ASCE)MT.1943-5533.0000548)
- Song, I., Suh, M., Woo, Y.-K., & Hao, T. (2004). Determination of the elastic modulus set of foliated rocks from ultrasonic velocity measurements. *Engineering Geology*, 72(3–4), 293–308. <https://doi.org/10.1016/j.enggeo.2003.10.003>
- Wang, L. (2011). *Mechanics of asphalt: Microstructure and micromechanics*. McGraw Hill.
- Wenk, H.-R., & Bulakh, A. (2004). *Minerals: Their constitution and origin*. Cambridge University Press.
- Yi, X., Chen, H., Wang, H., Tang, Z., Yang, J., & Wang, H. (2021). Cross-functional test to explore the determination method of meso-parameters in the discrete element model of asphalt mixtures. *Materials*, 14(19), <https://doi.org/10.3390/ma14195786>

- Yin, H. M., Buttlar, W. G., Paulino, G. H., & Di Benedetto, H. (2008). Assessment of existing micro-mechanical models for asphalt mastics considering viscoelastic effects. *Road Materials and Pavement Design*, 9(1), 31–57. <https://doi.org/10.1080/14680629.2008.9690106>
- You, Z, Adhikari, S, & Dai, Q. (2008). *Journal of Engineering Mechanics* (Vol. 134, pp. 1053–1063). ASCE.
- You, Z., & Dai, Q. (2007). Dynamic complex modulus predictions of hot-mix asphalt using a micromechanical-based finite element model. *Canadian Journal of Civil Engineering*, 34(12), 1519–1528. <https://doi.org/10.1139/L07-064>
- Zaoui, A. (2002). Continuum micromechanics: Survey. *Journal of Engineering Mechanics*, 128(8), 808–816. [https://doi.org/10.1061/\(ASCE\)0733-9399\(2002\)128:8\(808\)](https://doi.org/10.1061/(ASCE)0733-9399(2002)128:8(808))
- Zhang, H., Anupam, K., Scarpas, A., & Kasbergen, C. (2018). Comparison of different micromechanical models for predicting the effective properties of open graded mixes. *Transportation Research Record*, 2672(28), 404–415. <https://doi.org/10.1177/0361198118794713>